PAPER

A metamaterial-assisted coda wave interferometry method with nonlinear guided waves for local incipient damage monitoring in complex structures

To cite this article: Shengbo Shan *et al* 2024 *Smart Mater. Struct.* **33** 035017

View the article online for updates and enhancements.

You may also like

- Stochastic parameter estimation of heterogeneity from crosswell seismic data based on the Monte Carlo radiative transfer theory
Xiangcui Meng, Shangxu Wang, Genyang Tang et al.
- Coda Wave Interferometry Method Applied in Structural Monitoring to Assess Damage Evolution in Masonry and Concrete Structures
D Masera, P Bocca and A Grazzini
- Vibration-modelling-based fault feature analysis for incipient damage identification of sun gear
Xianzeng Liu

This content was downloaded from IP address 158.132.13.200 on 14/02/2024 at 01:17

IOP Publishing Smart Materials and Structures
Smart Mater. Struct. **33** (2024) 035017 (18pp) https://doi.org/10.1088/1361-665X/ad254c

A metamaterial-assisted coda wave interferometry method with nonlinear guided waves for local incipient damage monitoring in complex structures

Shengbo Shan[1,*], Ze Liu[2], Chi Zhang[1], Li Cheng[2,3,*] and Yongdong Pan[1]

[1] School of Aerospace Engineering and Applied Mechanics, Tongji University, Shanghai 200092, People's Republic of China
[2] Department of Mechanical Engineering, The Hong Kong Polytechnic University, Kowloon, Hong Kong
[3] Hong Kong Branch of National Rail Transit Electrification and Automation Engineering Technology Research Center, The Hong Kong Polytechnic University, Kowloon, Hong Kong

E-mail: shanshengbo@tongji.edu.cn and li.cheng@polyu.edu.hk

Received 1 November 2023, revised 29 December 2023
Accepted for publication 1 February 2024
Published 12 February 2024

Abstract

Nonlinear guided waves exhibit high sensitivity to material microstructural changes, thus attracting increasing attention for incipient damage monitoring applications. However, conventional nonlinear guided-wave-based methods suffer from two major deficiencies which hinder their applications: (1) mostly relying on the first arrivals of wave signals, they apply to limited inspection areas in simple structures in order to avoid wave reflections from structural discontinuities or boundaries; (2) they are prone to numerous deceptive nonlinear sources in the measurement system which might overwhelm damage-induced signal components. To tackle these challenges, we propose a metamaterial-assisted coda wave interferometry (CWI) method using second harmonic Lamb waves, applicable to the monitoring of local incipient damage in complex structures. Embracing the metamaterial concept, a so-called meta-screen is designed, whose geometry and layout can be flexibly tailored to target specific inspection zones in a structure. Capitalizing on its customized bandgap features, the proposed meta-screen allows for the passing of fundamental waves while preventing the second harmonic components generated by deceptive nonlinear sources from penetrating into the inspection area. Through numerical analyses on a plate with a rib stiffener, the efficacy of the meta-screen and the influence of occasional disturbance and regular pollution are evaluated. Experimental validations on an adhesive structure also confirm the superior sensitivity of the nonlinear coda waves to incipient damage, which is further enhanced by the deployment of the meta-screen alongside improved robustness against deceptive nonlinear sources outside the inspection area. The proposed metamaterial-assisted CWI method with second harmonic Lamb waves holds great promise for local incipient damage monitoring of complex structures.

Keywords: nonlinear guided waves, coda wave interferometry, metamaterial, incipient damage, complex structures

* Authors to whom any correspondence should be addressed.

© 2024 IOP Publishing Ltd

1. Introduction

Real-time and online monitoring of damage in engineering structures is crucial in various industrial applications like aerospace, nuclear, civil, and so on. One of the most challenging yet unsolved problems is the monitoring of weak and incipient damage before the initiation of any visible macro-scale defects, which is vital for maintenance decision makings [1]. Structural health monitoring (SHM) based on guided waves shows great promise for such applications owing to its high sensitivity to damage and the ability of the guided waves to reach large areas. Based on different wave-damage interaction mechanisms, guided-wave-based SHM techniques can be subcategorized into linear and nonlinear ones. Linear techniques use scattering waves for damage characterization. Their detection limit is confined by the wavelength which is typically in the macro scale (millimeter range) [2–4]. By contrast, nonlinear techniques rely on nonlinear guided waves which result from the interaction between the probing waves and material/structural microstructural defects. Nonlinear-guided-wave-based methods have been proven to inherently exhibit higher sensitivity to small and incipient damage in structures [5–7].

There exist various forms of nonlinear guided wave components, exemplified by higher harmonics [8–10] and mixed-frequency components [11, 12] depending on how primary waves in a nonlinear waveguide combine and interact. Specifically, second harmonic S0 mode Lamb waves feature a quasi-cumulative effect in the low-frequency range, i.e. their amplitude increases quasi-linearly with the propagation distance [13, 14]. This ultimately results in increased wave amplitudes to facilitate their measurement. Meanwhile, the quasi-cumulative effect is persistent within a rather wide low-frequency range, conducive to the frequency selection of the probing signals. With the second harmonic S0 mode Lamb waves, attempts were made to detect incipient damages like plasticity [15], fatigue [16], and thermal damage [17]. Most reported studies used the first arrivals in the Lamb wave signals. In practical applications, when the geometry of structures under inspection is complex, even the first arrivals may mix with the reflections from structural boundaries and discontinuities. As a result, these methods can only be applied to a limited small inspection area, which is away from structural irregularities and boundaries, thus hindering their application in complex structures.

Targeting the special need of SHM in complex structures, coda wave interferometry (CWI) technique has been developed, which characterizes damage with coda waves [18]. The concept of CWI was originally introduced by Snieder *et al* in seismic waves to evaluate the wave velocity changes in the ground [19]. A coda wave is considered to be a superposition of all scattered and reflected waves induced by defects and structural boundaries in a waveguide. A subtle change in the medium causes accumulated changes in coda waves, leading to a higher sensitivity of the CWI method than methods based on first arrivals [20–22]. Based on the CWI, various applications have been reported for the monitoring of different types of defects like weld fatigue crack [21], early-stage bolt looseness [23], corrosion [24], *etc.*

However, remaining under the umbrella of linear SHM technique, traditional CWI still suffers from the detection limit imposed by wavelength. To further enhance the sensitivity of CWI for incipient damage detection, an intuitive way is to combine the nonlinear guided waves and CWI, a topic that has not been exploited in the literature. Relevant to this, Smagin *et al* proposed a nonlinear CWI based on nonlinear pump-probe interaction induced by acoustic contact nonlinearity arising from local cracks in plates [25]. Qu *et al* further quantified the effect of the pump wave amplitude on crack detection with the nonlinear CWI method [26]. However, the method requires two physical channels to generate probe and pump waves. This might be challenging in some applications like the aerospace industry where there is a strict requirement for weight and reliability. An additional wave source will add weight and reduce the reliability of the whole system. In addition, these existing works on the nonlinear CWI focus on cracks. Therefore, developing a simpler yet feasible approach through combining nonlinear guided waves and CWI to cope with incipient damage in complex structures provides an alternative.

To tackle the problem, two important issues need to be considered. First, nonlinear guided waves generated by structural damage are usually weak and prone to various deceptive nonlinear sources in a measurement system. The disruptive effects of these nonlinear interferences should definitely be mitigated [1, 27]. Second, monitoring specific key and hot zones in a large structure is also needed in many practical applications. As coda waves contain multiple scattered and reflected waves through different paths over the structure, they inherently contain global and muffled information about the entire structure, thus compromising their sensitivity to local damage [28]. These issues may be potentially solved through tactic manipulation of the probing waves using metamaterials, which, upon a proper design, might offer properties that are absent in nature materials. In particular, metamaterials allow for customizing elastic waves in terms of wave filtering [29], steering [30], mode conversion [31], and so on. Relevant to the two aforementioned requirements, a few metamaterial designs were proposed in the literature. For example, surface-bonded metamaterial devices were designed to purify the second harmonic Lamb waves through wave filtering [32–35]. Through bandgaps tuning, a metamaterial device was proposed to trap guided waves of different frequencies in different zones [36]. Despite these successful attempts, the integration of the metamaterial design and CWI with nonlinear guided waves, the topic to be investigated in this paper, is still lacking.

Motivated by this, a nonlinear-guided-wave-based CWI method (NGW-CWI) assisted by metamaterials is proposed here to monitor local incipient damage in complex structures. This work shows a three-fold novelty. First, this is the first attempt to combine the CWI with time-domain second harmonic Lamb waves for incipient damage detection

in complex structures. Second, the effects of the deceptive nonlinear sources on CWI, unique to and detrimental to nonlinear-Lamb-wave-based methods, are apprehended and tackled. Third, recent advance in metamaterial design is embraced and integrated to enhance the performance of NGW-CWI towards more practical applications.

The outline of the paper is as follows. Section 2 introduces the concept of the proposed method. Numerical and experimental validations are carried out in sections 3 and 4 respectively to assess the method and demonstrate its efficacy for incipient damage in complex structures. Main conclusions are drawn in section 5.

2. Metamaterial-assisted nonlinear CWI

An NGW-CWI method, which shares the same philosophy as traditional CWI with linear guided waves, is proposed to monitor incipient damage in complex structures. The only difference is that the proposed NGW-CWI method leverages the time-domain signals of nonlinear guided waves while the traditional CWI uses linear waves. In this work, the second harmonic Lamb waves are used which are extracted with the phase-inverse method [1, 27]. By exciting Lamb waves in a weakly nonlinear plate with a pair of signals with inversed phases, the second harmonic response in the time domain $u_2(t)$ is obtained via

$$u_2(t) = \left(u_{1P}(t) + u_{1N}(t)\right)/2. \tag{1}$$

In the equation, $u_{1P}(t)$ and $u_{1N}(t)$ denote the responses to the pair of excitations with inversed phases where P and N are the notations of the positive and negative phase signs respectively. The subscripts 1 and 2 stand for the primary and second harmonic waves respectively. With the second harmonic responses from two subsequent measurements, denoted by the superscripts k-1 and k, a cross-correlation coefficient (CC) is defined as [36]

$$CC_2^k(\alpha,t) = \frac{\int_t^{t+T} u_2^{k-1}\left(t'(1+\alpha)\right) u_2^k(t')\,\mathrm{d}t'}{\sqrt{\int_t^{t+T}\left(u_2^{k-1}\left(t'(1+\alpha)\right)\right)^2\mathrm{d}t' \int_t^{t+T}\left(u_2^k(t')\right)^2\mathrm{d}t'}} \tag{2}$$

where t denotes the time and T is the window length for the calculation/measurement. Specifically, α is the stretching factor. The maximum value of CC occurs at the specific value α_k as

$$\alpha^k(t) = \arg\max_{\alpha}\left(CC_2^k(\alpha,t)\right). \tag{3}$$

As reported in the literature [37, 38], the temperature variation mainly changes the wave velocity (signal phase) while the damage severity significantly affects the wave amplitude. The use of the stretching factor enables one to analyze and mitigate the influence of temperature-variation-induce phase shift of the signals [24, 37, 39].

Finally, a decorrelation coefficient DI is proposed to quantify the changes in the response signals at a specific time t as

$$DI^k(t) = \left(1 - \max_{\alpha}\left(CC_2^k(\alpha,t)\right)\right) \times 100\%. \tag{4}$$

A larger DI indicates a higher possibility of damage occurrence, which is used for subsequent damage detection.

As mentioned above, NGW-CWI suffers from the interference of deceptive nonlinear sources in measurement systems. Meanwhile, the global nature of the wave propagation compromises the sensitivity of the NGW-CWI to local incipient damage. To tackle these issues, the concept of metamaterial is embedded into the NGW-CWI to customize/condition the guided waves before they reach the detection area as illustrated in figure 1. A so-called meta-screen is designed and installed onto the structure under inspection (referred to as host structure). The meta-screen can be tailored to cover a specific monitoring zone. The meta-screen allows for the passing of waves at the fundamental frequencies and prohibit the second-harmonic waves from passing through. Naturally, it also prevents any second harmonic waves generated by the outside nonlinear sources (including nonlinearities of measurement systems and outside damage) from penetrating into the inspection area while the damage-induced nonlinear waves are confined inside. In addition, the meta-screen also increases the interaction between the guide waves and the damage inside the inspection zone, thus enhancing the sensitivity of nonlinear coda waves to local incipient damage. The proposed methodology warrants the second harmonic signals received by the sensors which are enclosed by the meta-screen only stem from the interaction between the damage and the fundamental waves of the probing signals.

A general procedure is summarized to guide practical applications: (1) a monitoring zone is firstly determined for a given structure; (2) the unit cell of the meta-screen is designed according to the above-mentioned requirements on the passband and stopband; (3) the corresponding spatial layout of the meta-screen is designed to cover the monitoring zone; (4) the actuator is installed outside the monitoring zone while the sensor is installed inside; (5) with the captured signals, the DIs are calculated to monitor the health status of the zone.

Remarkably, although both second harmonic S0 and A0 mode waves may be generated in practice, we capitalize on the second harmonic S0 mode waves in the subsequent analyses for two reasons: (1) according to the theory, the fundamental A0 mode waves generate the second harmonic S0 mode waves and the mixing of fundamental A0 and S0 waves contributes to the second harmonic A0 mode waves [40]. However, both patterns cannot satisfy the internal-resonance condition for the cumulative second harmonic generation due to the dispersive nature of A0 mode waves. By contrast, the S0 mode waves in the low-frequency range can approximately satisfy the internal-resonant condition to generate the cumulative second harmonic S0 mode waves. Therefore, the second harmonic S0 mode waves generated by the fundamental S0 mode waves should be dominant in the captured second harmonic

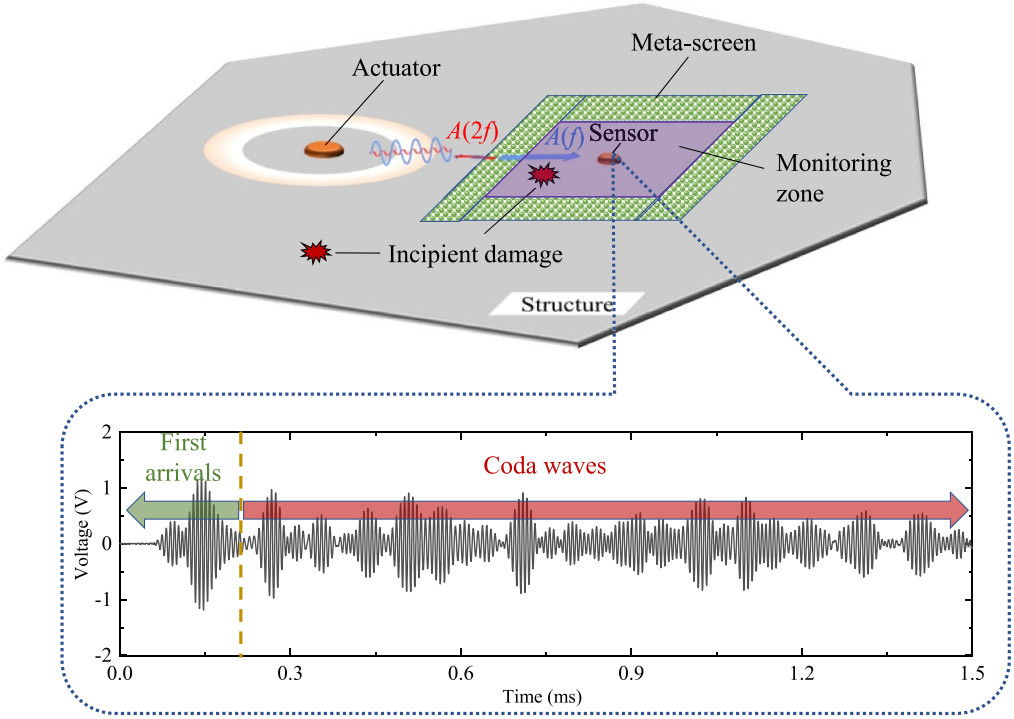

Figure 1. Concept of the metamaterial-assisted nonlinear coda wave interferometry method.

responses. (2) The proposed NGW-CWI method utilizes the full bandgap of the designed meta-screen. The second harmonic A0 mode Lamb waves, if generated outside the meta-screen, are blocked. The fundamental A0 mode Lamb waves penetrating into the monitoring zone can also interact with the incipient damage to generate the second harmonic Lamb waves, albeit without the cumulative effect. Such interaction is also beneficial to damage monitoring. Therefore, the presence of the A0 mode wave will not be a problem for the proposed method. Details of the meta-screen design and layout will be introduced in the subsequent sections considering specific SHM cases.

3. Numerical examples and concept validation

3.1. Design of the meta-screen

A 2 mm thick aluminum plate with rib stiffeners is taken as a representative example, to which a meta-screen and the proposed NGW-CWI are applied. The meta-screen is empirically designed based on the bandgap principles of periodic phononic crystals. As a rule of thumb, the lattice constant should be comparable to the wavelength. This work focuses on the low-frequency range (50 kHz–300 kHz), where the wavelengths of Lamb waves range approximately from 5 mm to 100 mm. In addition, a smaller lattice constant is preferred in practice as it leads to a lighter and smaller meta-screen. Therefore, the lattice constant is restricted to the millimeter range. Following the designs presented in the literature [29, 32, 41], we meticulously tune the lattice constant and other geometric parameters of the meta-screen to evaluate the resultant band structures. As the end of the process, we achieved the design with a satisfactory bandgap with the unit cell shown in figure 2(a). The meta-screen, in form of a few periodically arranged lead patches, is bonded on the plate through the adhesive layer. The lattice constants in both x and y directions are set to 4 mm. The thickness of the bonding layer is 0.05 mm. The lead patch contains a 0.5 mm thick uniform base and a $2 \times 2 \times 2$ mm^3 cubic scatterer. The base is designed for the ease of installation while the cubic scatterer alongside the rest of structural components generates bandgaps for the manipulation/conditioning of the incoming waves. Lead is selected for the meta-screen owing to its drastic property difference with aluminum, conducive to bandgap generation. Meanwhile, meta-screens made of lead can be more easily fabricated, which are therefore widely used in existing laboratory concept-of-proof studies [31, 41]. It is worth noting that we have also developed a topological optimization tool for metamaterial design that targets more complex requirements and applications [35]. As this work aims to demonstrate the concept of NGW-CWI, we believe that the empirical design is sufficient to meet the requirements.

The band structure of the unit cell is calculated using COMSOL Multiphysics. Material parameters for the three components are tabulated in table 1 in terms of mass density ρ, Young's modulus E, and Poisson's ratio v. A sufficiently refined mesh (0.01 mm in length) is used to ensure the accuracy of the calculation. The Bloch-Floquet boundary condition is applied in both x and y directions. Considering the periodicity in the x and y direction, the corresponding irreducible

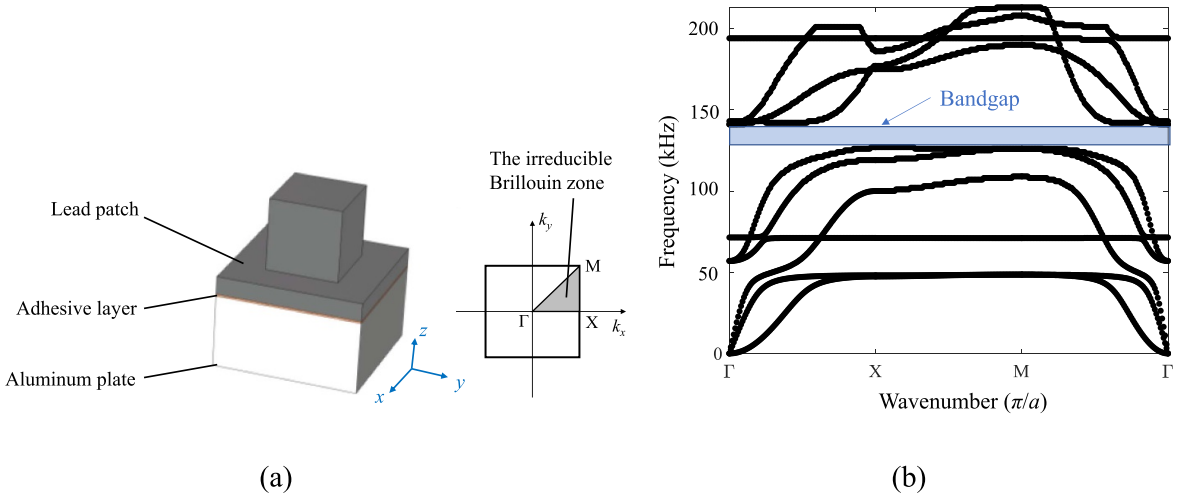

Figure 2. (a) Unit cell of the meta-screen with the corresponding irreducible Brillouin zone and (b) band structure.

Table 1. Material parameters of the aluminum, adhesive and lead.

	ρ (kg m^{-3})	E (GPa)	v
Aluminum	2700	70	0.33
Adhesive	1080	1.31	0.4
Lead	11 370	16	0.42

Brillouin zone is shown in figure 2(a). The coordinates of the three points Γ, X, and M in the wavenumber space are (0, 0), (π/a, 0), and (π/a, π/a) respectively, with a being the lattice constant. By sweeping the wave number k along the edges of the irreducible Brillouin zone (Γ-X, X-M and M-Γ as the x-axis in figure 2(b)) and searching for eigen frequencies f, the band structure is obtained and shown in figure 2(b). Each curve in the band structure corresponds to a propagating wave mode. Therefore, a complete bandgap (129–141 kHz) is observed. If the frequency of guided waves falls into the bandgap, they cannot pass through the meta-screen.

3.2. *Finite-element model for validation*

The performance of the designed meta-screen is assessed with time-domain simulations. A finite element model is built in Abaqus/Explicit as illustrated in figure 3(a). The meta-screen is bonded on the surface of a stiffened aluminum plate with a 0.05 mm thick adhesive layer. The stiffener, also made of aluminum, is rigidly bonded on the plate, which is realized by the 'tie' constraint in Abaqus. The thickness of the two panels in the 'T'-shaped stiffener is 1 mm and its other geometric parameters are illustrated in figure 3(b). The stiffened plate is used as a representative complex structure in the simulations to show the feasibility of the proposed method as the stiffener causes wave reflection and scattering and makes the wave propagation more complex. The meta-screen includes four rectangular patches (based on the above design) to cover a monitoring area of 57 mm × 57 mm. Specifically, there is a 1 mm-gap between the patches to mimic the imperfect installation in practical applications. Each lead patch contains 6 and 20 unit cells in the two directions, respectively. It is worth noting the reason for using four independent patches instead of one single integrated one is to show the flexibility of the proposed method to cope with different monitoring zones of interest with customizable configuration. The geometry of the finite element model is sketched in figure 3(b) with detailed dimensions. An excitation is applied on the top surface along the left edge of the plate with a prescribed displacement in the z direction with an amplitude of 0.5 μm. Tone burst signals, windowed by the Hann function ($E(t)$), are used as excitation, defined by

$$E(t) = \left(1 - \cos\left(\frac{2\pi f}{N}t\right)\right)\sin(2\pi f t) \tag{5}$$

where f and N denote the central frequency and the number of cycles, respectively. In the simulations, f is set to 70 and 140 kHz with their corresponding N as 7 and 14 respectively to guarantee the same duration of the two excitations. The meta-screen and the bonding layer are assumed to be linear in elasticity whose parameters can be referred to table 1. By contrast, the aluminum plate has nonlinear elastic properties. The nonlinear elastic behavior is characterized with the Landau–Lifshitz model as

$$\begin{aligned}\mathbf{T}^{RR} = {} & \lambda \,\mathrm{tr}\left[\mathbf{E}\right]\mathbf{I} + 2\mu\mathbf{E} + \bar{A}\mathbf{E}^2 + \bar{B}\,\mathrm{tr}\left[\mathbf{E}^2\right]\mathbf{I} \\ & + 2\bar{B}\,\mathrm{tr}\left[\mathbf{E}\right]\mathbf{E} + \bar{C}(\mathrm{tr}\left[\mathbf{E}\right])^2\mathbf{I}\end{aligned} \tag{6}$$

where $\mathbf{T}^{RR}$ is the second Piola-Kirchhoff stress tensor and $\mathbf{E}$ is the Lagrangian strain tensor. λ and μ are the Lamé constants. $\bar{A}$, $\bar{B}$, and $\bar{C}$ are the Landau constants as −351.2 GPa, −140.4 GPa and, −102.8 GPa respectively for aluminum [40, 42]. The operation tr[] denotes the trace of a matrix. The tensor $\mathbf{I}$ is an identity tensor. Accordingly, a user material subroutine named VUMAT is used in Abaqus/Explicit to characterize the nonlinear elasticity of the material. The in-plane displacement in the z direction (Uz) at an arbitrarily-selected position (27 mm away from the damage zone as shown in figure 3(b))

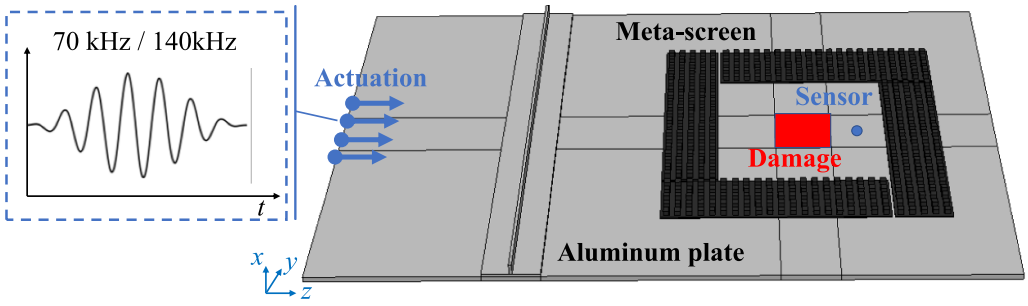

(a)

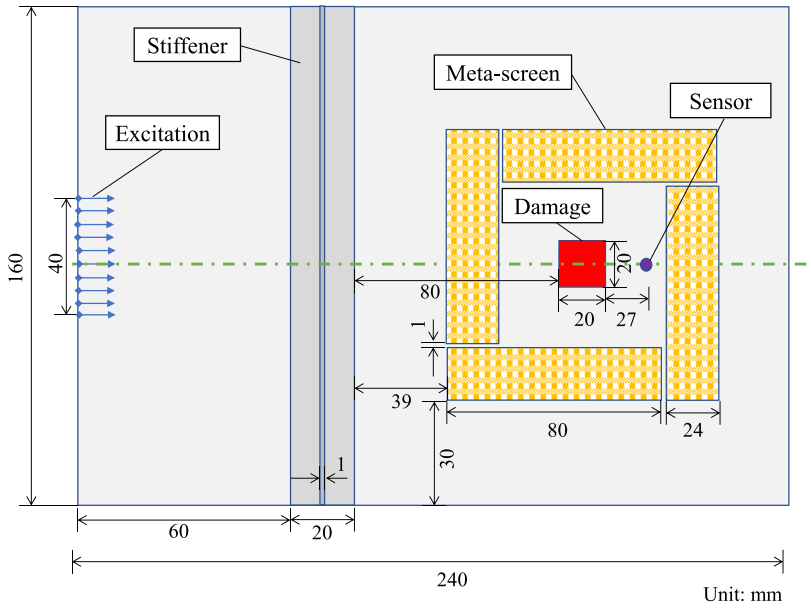

(b)

Figure 3. (a) Sketch and (b) dimensions of the finite element model.

in the monitoring zone is extracted as the sensor output. The sampling frequency of the system is 10 MHz.

3.3. Enhanced damage detection sensitivity

The wave-filtering ability of the meta-screen is first assessed. By respectively setting the central frequencies of the tone burst signals at 70 kHz and 140 kHz, the primary wave fields in terms of magnitude of displacement (U, magnitude) at 160 μs at the two frequencies before and after the installation of the meta-screen are compared in figure 4. The group velocities of S0 mode waves at 70 kHz and 140 kHz in the plate are very close: 5411 m s^{-1} and 5398 m s^{-1} respectively. Therefore, a propagation time of 160 μs corresponds to a propagation distance of about 0.86 m, which is much larger than the length of the plate (0.24 m). Therefore, the resulting wave field contains various reflections from the boundaries. Results show that the 70 kHz waves can penetrate into the monitoring area while the 140 kHz waves are blocked by the meta-screen to the outside area, which has also been confirmed by scrutinizing the wave propagation process in the simulations. This agrees well with the passband and stopband of the designed meta-screen, which proves that the meta-screen meets the requirement for wave manipulation before its further integration with NGW-CWI.

Using the meta-screen, a 20 mm $\times$ 20 mm local incipient damage is introduced to the plate as illustrated in figure 3(b), which is simulated by tripling the Landau constants ($\bar{A}$, $\bar{B}$, and $\bar{C}$) of the material in the local area [40, 42]. It is worth noting that the stiffened plate has weak nonlinear elastic properties and the damage is simulated by amplifying the nonlinear elastic constants in local zones. The overall responses captured by the sensor before and after the introduction of the damage are shown in figure 5(a). Due to the dominance of the linear wave components, the overall responses are referred to as linear wave responses hereafter. It can be seen that the linear waves hardly change after the incipient damage is introduced.

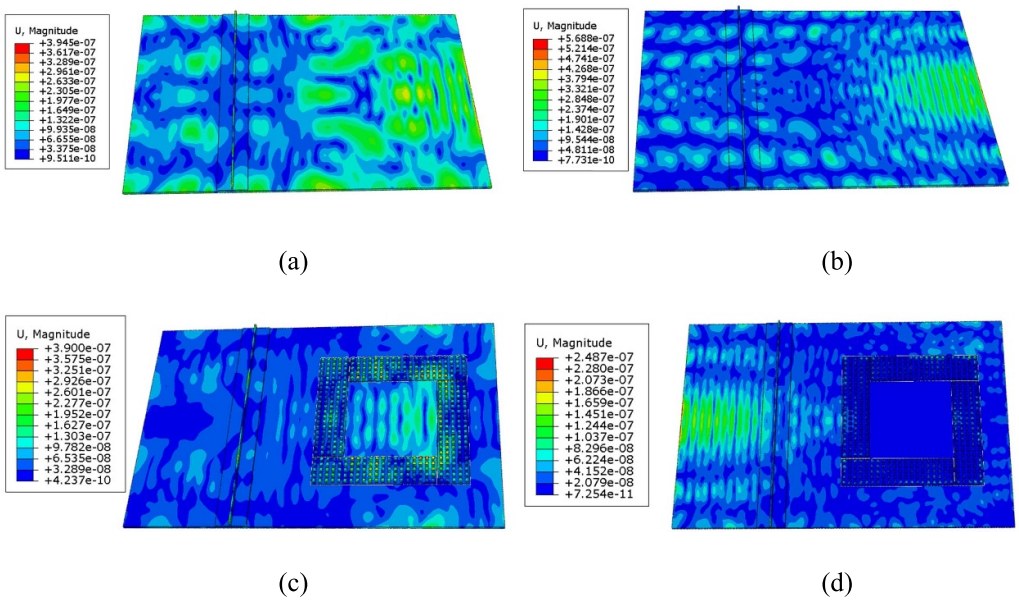

Figure 4. Wavefields of Lamb waves in terms of the magnitude of displacement (U, magnitude) at 160 μs under different conditions: (a) 70 kHz excitation without the meta-screen; (b) 140 kHz excitation without the meta-screen; (c) 70 kHz excitation with the meta-screen; (d) 140 kHz excitation with the meta-screen.

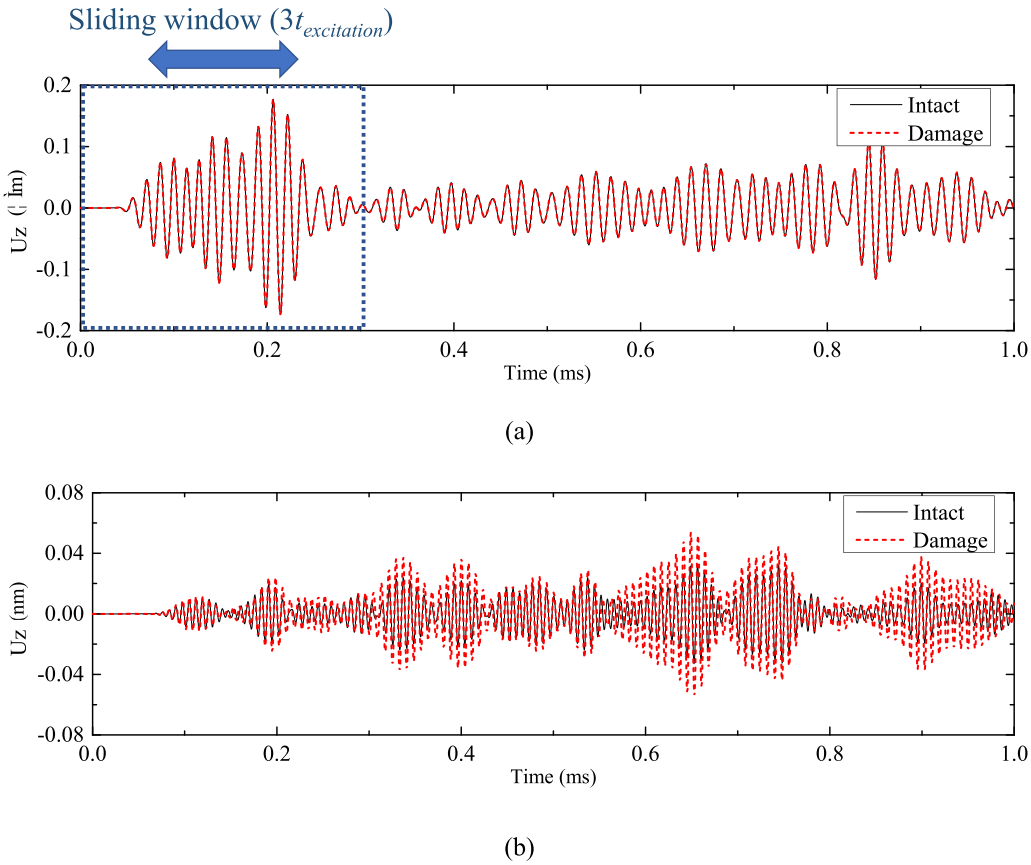

Figure 5. (a) Linear and (b) nonlinear responses of Lamb wave signals received by the sensor in terms of the displacement in z direction (Uz) before and after the introduction of damage when the meta-screen is installed.

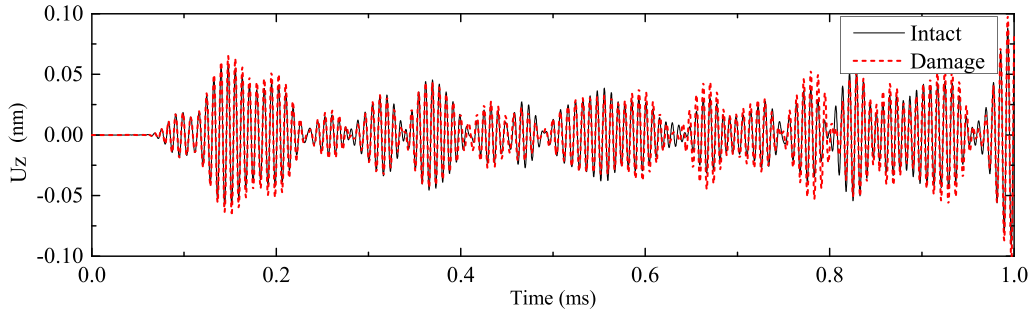

Figure 6. Nonlinear responses of Lamb wave signals received by the sensor before and after the introduction of damage when the meta-screen is not installed.

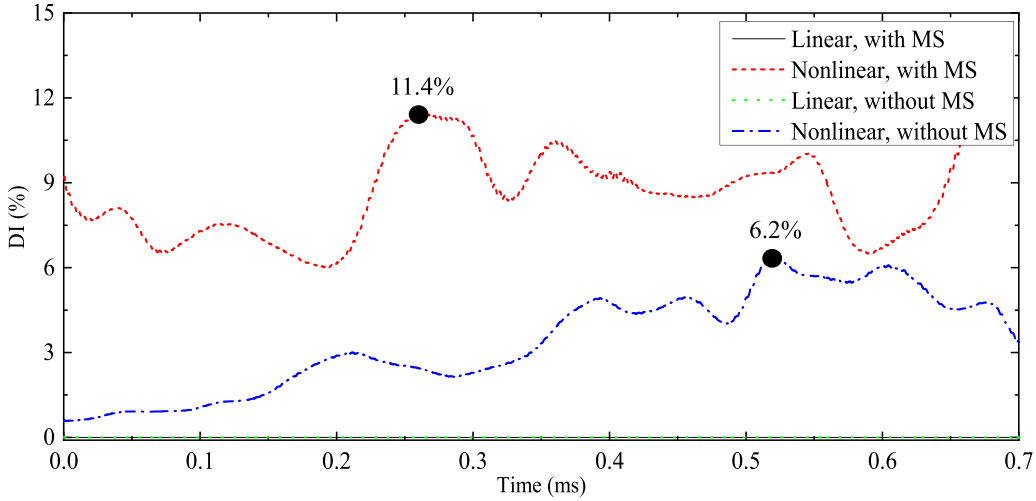

Figure 7. Calculated *DI*s with the linear and nonlinear Lamb wave signals measured in the system with/without the meta-screen (MS).

The nonlinear waves are then extracted with the phase-inverse method, with the results shown in figure 5(b). Significant change in the nonlinear waves is observed, especially for the coda waves.

By comparison, the same simulation is conducted when the meta-screen is absent. With the introduction of the same incipient damage, the linear wave hardly changes (not shown) but nonlinear coda waves are significantly affected as shown in figure 6. Compared with figure 5(b), the nonlinear coda waves are less altered by the damage in the absence of the meta-screen.

To quantify the changes in the linear and nonlinear coda waves, the *DI*s are calculated. Two important parameters have to be determined as the window length and the whole signal length respectively. A large window length reduces the sensitivity of the damage detection due to a wider coverage of wave packets and more averaged information for the correlation analysis. By contrast, a small large window may cause an over-amplification of the signal differences so that the robustness against measurement noise is adversely affected. The selection of the whole signal length depends on the wave attenuation during propagation. The attenuation of the Lamb waves during propagation affects the coda waves in terms of the signal-to-noise ratio. The coda waves corresponding to a large whole signal length with low signal-to-noise ratio will significantly reduce the accuracy of damage detection. By contrast, a too small whole signal length may not capture adequate coda wave information for damage detection. In the present work, the metallic plates are considered in which the wave attenuation during propagation is deemed relatively low. A $3t_{\text{excitation}}$-$10t_{\text{excitation}}$ criteria is adopted to choose the window length ($3t_{\text{excitation}}$) and the whole signal length ($10t_{\text{excitation}}$) respectively, with demonstrated effectiveness in our previous work [36]. The $t_{\text{excitation}}$ is the duration of the excitation signal, which is 0.1 ms in this case. An example of window length is illustrated in figure 5(a). The total signal length is 1 ms in the simulations, corresponding to a propagation distance of about 5.4 m which is much larger than the length of the plate (0.24 m). Therefore, the resulting waves should contain reflections from the boundaries, all contributing to the collected coda waves.

Before and after the introduction of the incipient damage, the *DI*s are calculated and shown in figure 7. The *DI*s for the linear waves are extremely low (less than 0.5%) no matter whether the meta-screen is installed or

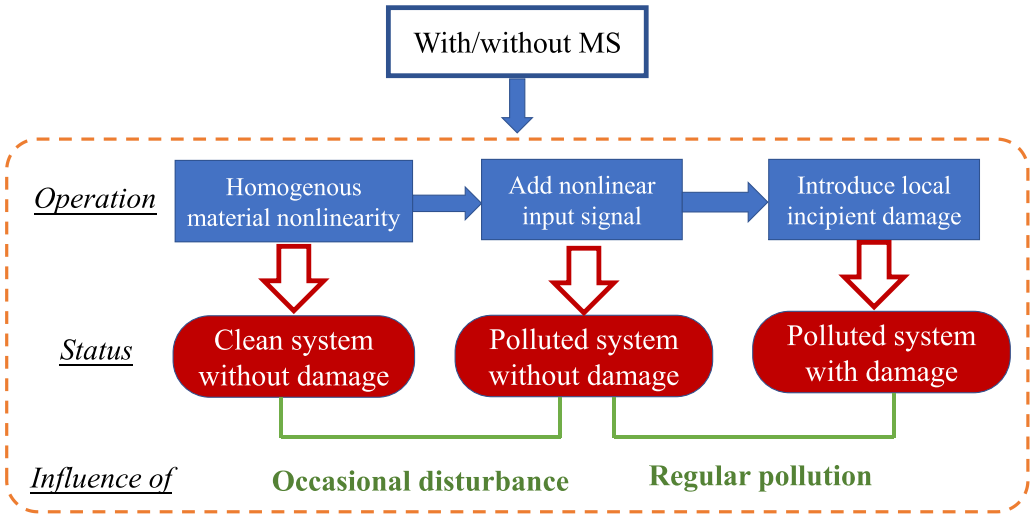

Figure 8. Procedure to demonstrate the robustness of the proposed method against deceptive nonlinear sources in finite element simulations.

not. By comparison, the nonlinear coda waves are much sensitive to the same incipient damage. More specifically, the maximum value of *DI* of nonlinear waves without the meta-screen is about 6.2%, increased to a much higher value (11.4%) with the deployment of the meta-screen. This demonstrates the higher sensitivity of the proposed NGW-CWI over the traditional CWI with linear guided waves. Meanwhile, the sensitivity of the nonlinear coda waves to local incipient damage is significantly enhanced by the meta-screen.

3.4. Robustness against occasional disturbance and regular pollution

The robustness of the proposed method against nonlinear interferences is further evaluated with the process illustrated in figure 8. Generally, there are two types of deceptive nonlinear sources, namely the occasional disturbance and regular pollution respectively. The former occasionally takes place during the service of the structure such as the occurrence of an incipient damage outside the monitoring zone. The latter inherently exists in the system exemplified by the nonlinearity of the instrumentation.

First, the influence of the occasional disturbance is evaluated. Without special considerations on the positions of the disturbance outside the monitoring zone, the occasional disturbance is simply simulated by adding a 14-cycle tone burst signal of 140 kHz to a primary 70 kHz excitation signal of 7 cycles. The amplitude of the added 140 kHz signal is 1% of the 70 kHz signal. For an intact plate, the linear and nonlinear responses before and after the introduction of the occasional disturbance are compared. Both systems, with/without the meta-screen, are tested and the resultant *DI*s are shown in figure 9(a). It follows that the linear responses are less sensitive to such disturbance while the nonlinear waves are severely affected. The nonlinear waves captured in the system without the meta-screen are more vulnerable to such occasional disturbance. Specifically, the maximum value of *DI* reaches 40% in the system without the meta-screen while it is 14% in the system with the meta-screen. This proves one of the beneficial features of the proposed method in minimizing occasional disturbance outside the screened area in the structure.

The robustness of the proposed method against regular pollution is then examined. If the nonlinearity is generated in the instrument (especially in the power amplifier), it results in a distortion of the excitation signal applied to the actuator. The nonlinear wave components generated by the actuator should propagate independently with the linear waves. To mimic the polluted system by regular instrumentation nonlinearity, the same 140 kHz signal is added in the primary excitation signal. The local incipient damage in the monitoring zone as described above is then introduced. Similarly, for both systems, with and without the meta-screen, the corresponding *DI*s are compared in figure 9(b). It is worth noting a 'thickness' is observed in the obtained curves of *DI*s. This is caused by the sliding of the window when calculating *DI*s. When local changes in the signals are large, *DI*s may become 'unstable' with oscillations as the window slides, resulting in the 'thickness'-like feature. A longer window length can smoothen the curves at the expense of reducing the damage detection sensitivity. Since the oscillations do not affect the variation trend, we keep the window length as $3t_{\text{excitaion}}$ in the analyses. Results show that the system with the meta-screen is more sensitive to incipient damage. In addition, due to the pollution of the system, the maximum *DI* of the nonlinear waves in the system with meta-screen decreases from 11.4% to 7%. However, for the

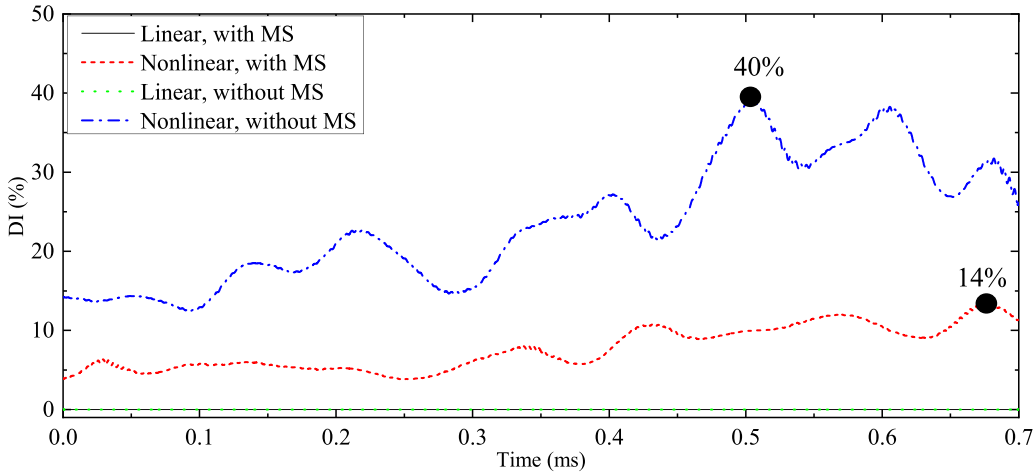

(a)

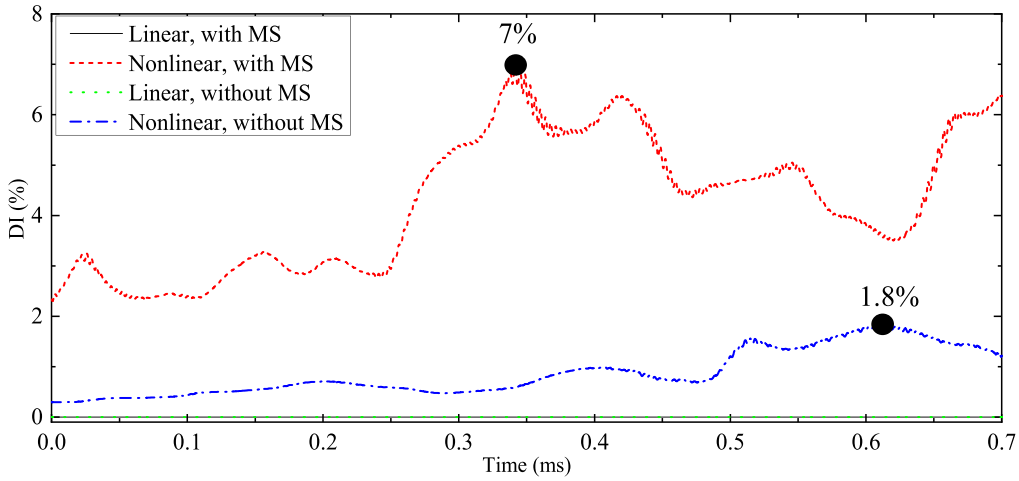

(b)

Figure 9. Calculated *DI*s with the linear and nonlinear Lamb wave signals when the (a) occasional disturbance and (b) regular pollution is introduced.

system without the meta-screen, the maximum *DI* significantly drops from 6.2% to 1.8%. This indicates that the meta-screen indeed entails enhanced robustness against regular pollutions.

It is worth noting that the nonlinearity of the designed meta-screen is not taken into consideration in the simulations which may have an impact on the nonlinear coda waves. The reasons for this are explained as follows: (1) when considering the nonlinearity of the meta-screen, the nonlinear coda waves captured by the sensor will then reflect the changes in both the original monitoring zone and the meta-screen, resulting in ab enlarged monitoring zone. In this case, the corresponding second harmonic Lamb waves outside the enlarged monitoring zone will still be blocked. Since the properties of the meta-screen does not change during the inspection, captured changes in the nonlinear coda waves can be still attributed to the damage incurred inside the monitoring zone. Therefore, the advantages of the proposed method persist even in the presence of the nonlinearity of the meta-screen. (2) In this work, aluminum and lead are used for the monitoring structure and meta-screen, respectively, as a proof-of-concept demonstration of the NGW-CWI. In practice, we can flexibly choose a weaker nonlinear material to design the meta-screen to mitigate its influence, which will be systematically considered in our future work.

As a summary, the proposed meta-screen-assisted NGW-CWI method is validated numerically. Comparing with the traditional CWI with linear Lamb waves, the NGW-CWI shows much increased sensitivity to local incipient damage. With the aid of the meta-screen, the performance of the NGW-CWI can be significantly improved. Specifically, the meta-screen forces the CWI to 'focus' on the monitoring zone through two main channels. Firstly, the additional wave reflections from the meta-screen cause the coda waves to interact more intensively with the internal damage, thus increasing the energy level of the signal and consequently the sensitivity of the CWI to damage. Meanwhile, as the deceptive nonlinear interference caused by regular pollution can be filtered out by the meta-screen, the nonlinear waves inside the monitoring zone are more closely related to the material nonlinearity. This also leads to an increased sensitivity of the CWI. Secondly, anomalies (occasional disturbance) outside the monitoring zone have less influence on the monitoring inside the zone since the second harmonic Lamb waves generated outside the monitoring zone are blocked.

4. Experimental investigations

Experiments are conducted to further validate the proposed method on a 2 mm-thick aluminum plate as shown in figure 10. Two small aluminum patches (30 mm × 30 mm × 2 mm) are bonded using adhesive onto the corners of the plate to mimic a complex adhesive structure. A PZT actuator of 30 mm × 30 mm × 0.5 mm is bonded at the center of the plate for wave actuation and two small PZT sensors (5 mm × 5 mm × 0.5 mm) are installed for wave reception. The previously designed meta-screen is manufactured as a single entity by CNC (computer numerical control) machining. The geometry of the designed meta-screen is relatively simple, requiring only the cutting of corresponding horizonal and vertical slots on a lead plate. The meta-screen contains two units covering a monitoring area of 136 mm × 160 mm at the corner of the plate. The selection of the corner as detection area is to further showcase the appealing features of the proposed method to monitor an area with complex wave propagating characteristics. In addition, it is easier to artificially produce local incipient damages at the corners in practice for the validation of the proposed method. The PZTs, meta-screen and the two aluminum patches are bonded on the plate with the UHU 2-component epoxy. Such configuration allows one to evaluate the performance of the meta-screen by cross-checking the responses from the two sensors. The geometry of the specimen is sketched in figure 10(b).

Note that a different configuration is considered in the experiments from the one used in the simulation. As coda waves result from various wave propagation paths, a slight difference between the system configurations used in the simulation and the experiments (such as transducer positions, material properties, wave excitation patterns, etc.) would cause significant discrepancies in the simulation of coda wave signals. It is therefore extremely difficult to build a finite element model to ensure that the time-domain coda wave signals in the simulations match those in the experiments. Most importantly, the simulations are intended to show the feasibility of the proposed method for incipient damage monitoring, rather than to offer a predictive numerical tool for prediction/duplicate experiments. Therefore, we chose a stiffened plate in the simulations and a bonded plate in the experiments as two representative structures to validate the proposed method from different perspectives.

The measurement system works as follows. The waveform generator outputs an excitation signal to the RITEC GA-2500A power amplifier. The excitation signal is amplified to 200 V and then applied to the PZT actuator. The generated guided waves are finally captured by the PZT sensors and stored in the oscilloscope. The experimental procedure is designed in figure 10(c). The signals are first captured on the bare plate as the reference. Test is carried out again after the installation of the meta-screen to assess its wave screening ability. After that, a local incipient damage is created in the monitoring zone (Damage 1) to validate the efficacy of the NGW-CWI method. Finally, a similar damage is introduced to the plate outside the monitoring zone (Damage 2) to assess the robustness of the proposed metamaterial-assisted NGW-CWI method against other nonlinear sources outside the inspection area.

Following the procedure, responses of Sensor 1 to the 70 kHz and 140 kHz excitations are compared before and after the installation of the meta-screen as shown in figure 11. Specifically, the number of cycles is set to 10 for both excitations. Results show that the 70 kHz Lamb waves are less affected by the meta-screen while the 140 kHz waves are significantly attenuated, which agrees with the expected band structure of the proposed meta-screen design (140 kHz in the stopband and 70 kHz in the passband), although only a limited number of unit cells are used. A transmission ratio (TR) is defined to further quantify the effect of the meta-screen as

$$\mathrm{TR} = \frac{\sqrt{\int_0^{10t_{\mathrm{excitation}}} \left(x_{\mathrm{withMS}}(t)\right)^2 \mathrm{d}t}}{\sqrt{\int_0^{10t_{\mathrm{excitation}}} \left(x_{\mathrm{withoutMS}}(t)\right)^2 \mathrm{d}t}} \tag{7}$$

where $x_{\mathrm{withoutMS}}(t)$ and $x_{\mathrm{withMS}}(t)$ are the signals from the same sensor before and the after the installation of the meta-screen. The TRs induced by the meta-screen for the linear waves at

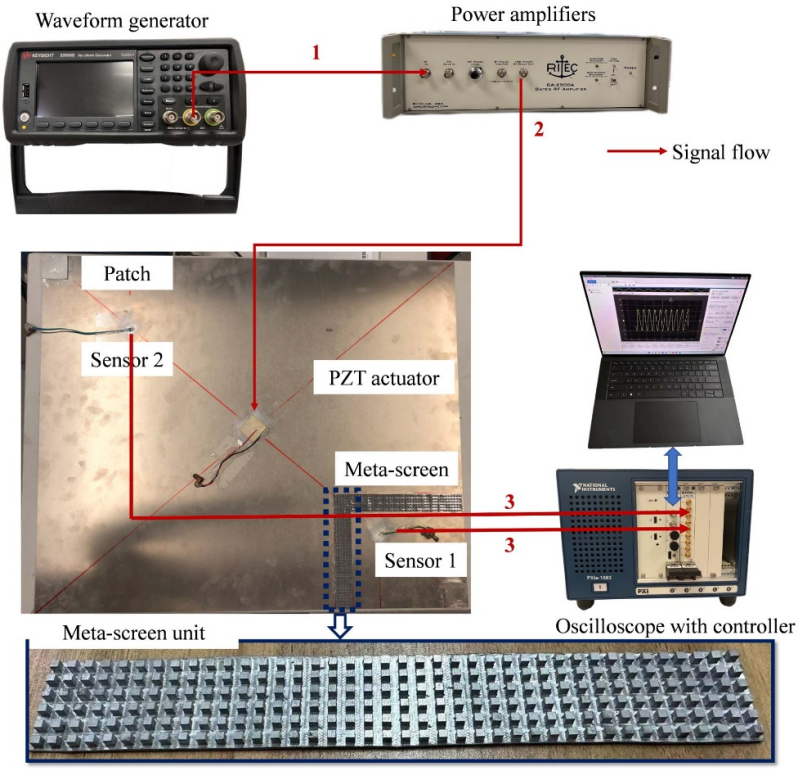

(a)

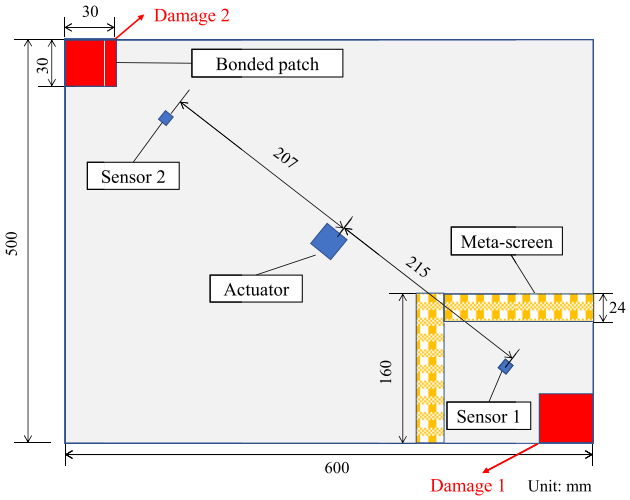

(b)

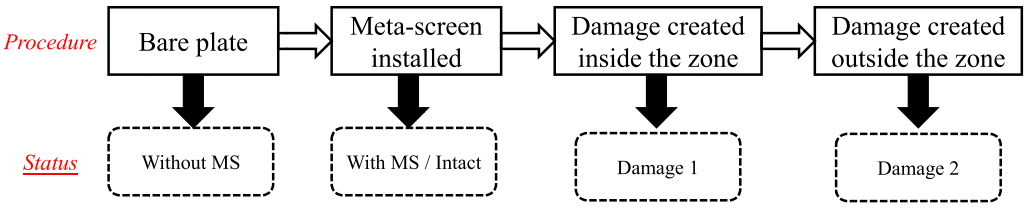

(c)

Figure 10. Experimental set-up: (a) the measurement system, (b) sketch of the specimen; and (c) the procedure of testing.

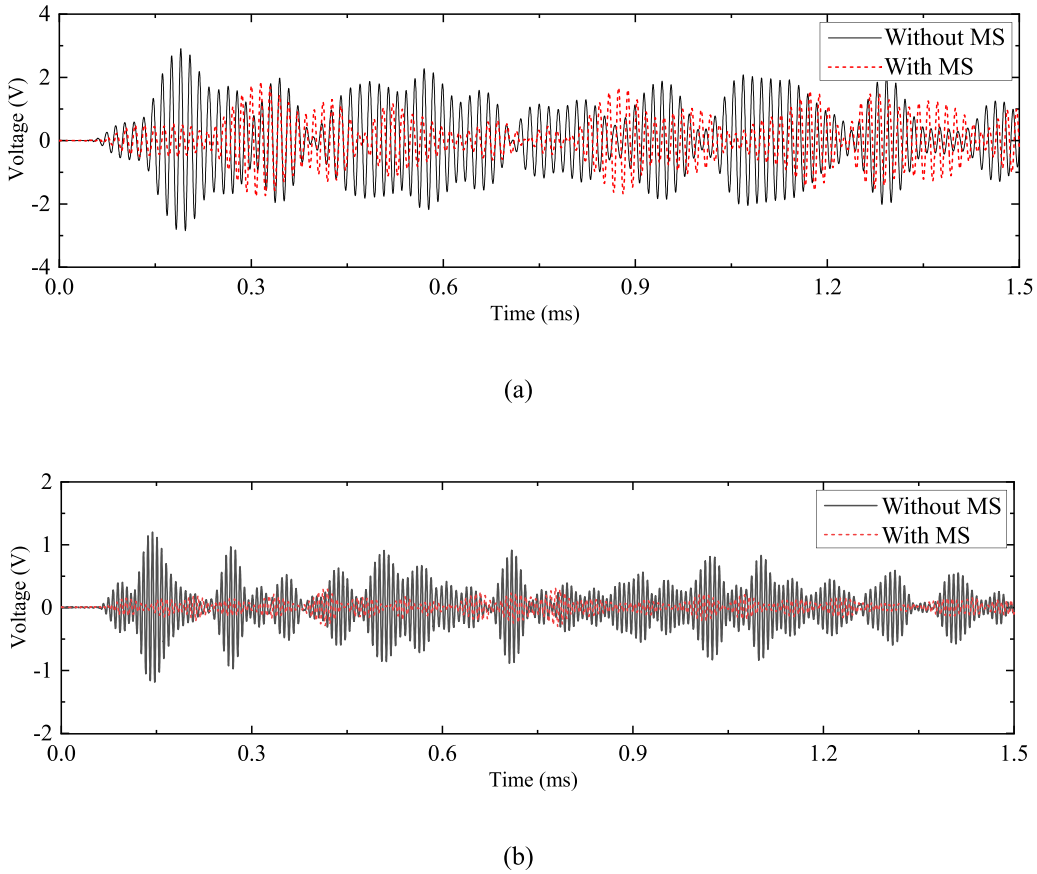

Figure 11. Responses of Sensor 1 before and after the installation of the meta-screen at (a) 70 kHz and (b) 140 kHz.

70 kHz and 140 kHz shown in figure 11 are 0.65 and 0.28, respectively.

After that, by setting the excitation frequency at 70 kHz, the phase-inverse method is used to extract the nonlinear responses with a representative nonlinear response of Sensor 1 shown in figure 12(a). Due to the uncertainty in the measurement system and noise, various components at other frequencies also exist apart from the second harmonic components. Therefore, a Butterworth filter is designed to separate the second harmonic components with the results shown in figure 12(b). The fast Fourier transform is applied to the original and filtered signals and their spectra are shown in figure 12(c). Note that a strong component at about 15 kHz is observed in the original spectrum. This may be caused by the nonlinear static component considering the dynamics of the piezoelectric sensor, which deserves to be further investigated in future work. Have said that, the designed filter effectively preserves the second harmonic responses in the time domain, which will be used in the subsequent analyses.

The second harmonic responses of Sensor 1 are then extracted before and after the installation of the meta-screen as shown in figure 13. The amplitude of the second harmonic responses decreases significantly after the installation of the meta-scree with the corresponding TR being 0.31.

This reveals that nonlinear waves generated outside the monitoring zone is more dominant than the nonlinear waves inside, which indicates the strong regular pollution in the system.

After that, an incipient damage is introduced to the bonding layer under the aluminum patch in the monitoring zone. The system is in the stage of 'Damage 1'. The creation of the damage is achieved by a thermal aging treatment to the patch at 60 °C for an hour, which has been proven to be effective to create microstructural changes in the epoxy [43] used as adhesive. The linear and nonlinear responses in the stages of 'Intact' and 'Damage 1' are compared with the representative time-domain signals received by Sensor 1 shown in figure 14. While the linear waves are very slightly affected by the damage (figure 14(a)), the nonlinear waves experience remarkable changes to the incipient damage (figure 14(b)). Meanwhile, the coda part of the nonlinear signal also presents higher sensitivity than the first several wave packets. Correspondingly, the *DI*s are calculated with the responses before and after the introduction of Damage 1 following the $3t_{\text{excitation}}$-$10t_{\text{excitation}}$ criteria [36] in figure 15. The corresponding total signal length is therefore 1.5 ms in the experiments, corresponding to a

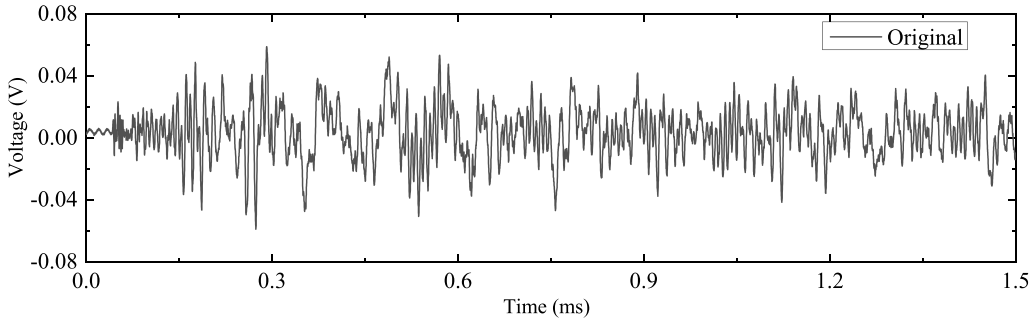

(a)

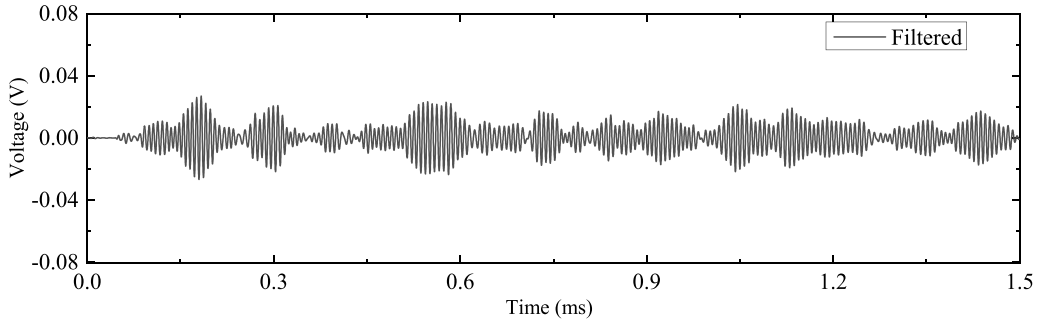

(b)

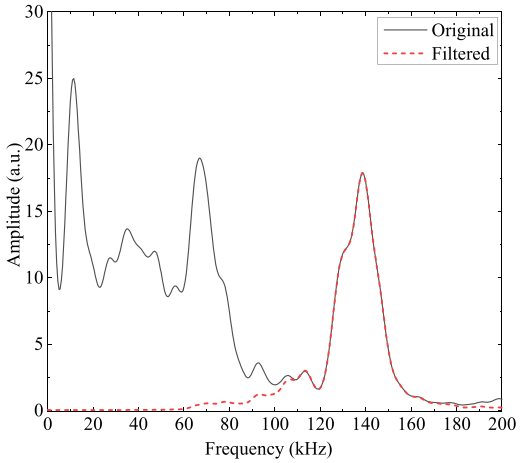

(c)

Figure 12. (a) Extracted nonlinear wave signal received by Sensor 1 at 70 kHz; (b) filtered nonlinear signal; (c) spectra of the original and filtered nonlinear responses.

propagation distance of about 8.1 m. The maximum value of *DI* for nonlinear waves from Sensor 1(22%) is much larger than that from Sensor 2 (9.8%), showing the enhanced sensitivity of the NGW-CWI to local incipient damage by the meta-screen.

Finally, a similar damage is introduced to the bonding layer under the patch outside the monitoring zone to simulate occasional disturbance and the system is in the stage of 'Damage 2'. The bonding layer is heated at the same temperature for the same duration as the above case. As

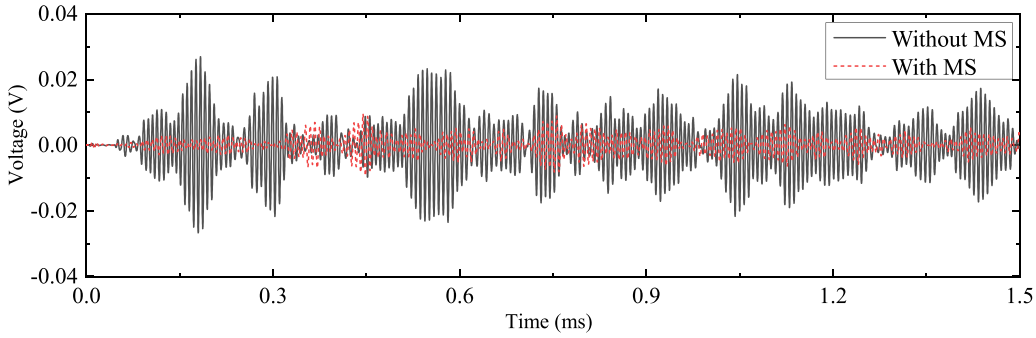

Figure 13. Extracted nonlinear wave signals received by Sensor 1 at 70 kHz before and after the meta-screen is installed.

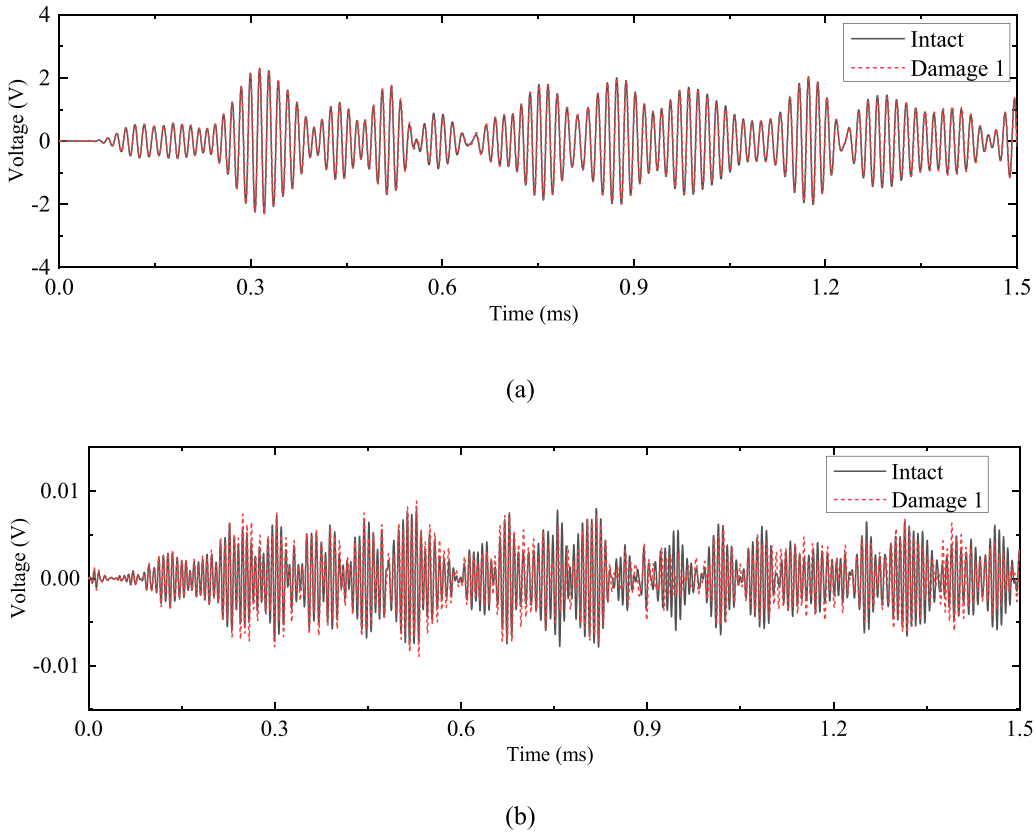

Figure 14. Responses of Sensor 1: (a) linear and (b) nonlinear, before and after Damage 1 is introduced inside the monitoring zone.

a representative case, the nonlinear signals of Sensor 1 in the stages of 'Damage 1' and 'Damage 2' are presented in figure 16(a), which shows very slight change in the nonlinear responses. The *DI*s for the linear and nonlinear waves captured by both ensors are obtained in figure 16(b). The maximum *DI* for the nonlinear waves at Sensor 1 (3.2%) is much smaller than that at Sensor 2 (6.2%). This indicates that the second harmonic Lamb waves inside the monitoring zone covered by the meta-screen is less affected by the outside disturbance, which demonstrates the robustness of the proposed method. To this end, the proposed method has been firmly confirmed experimentally.

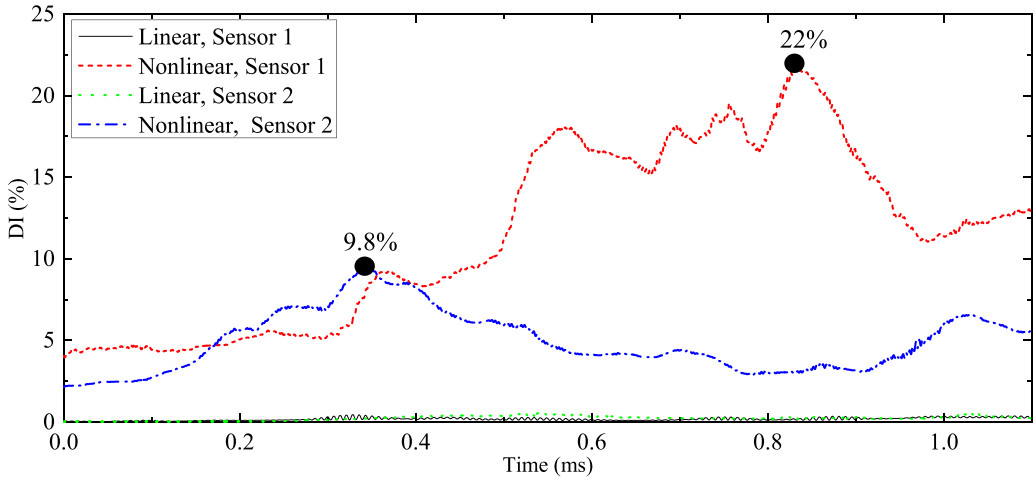

Figure 15. Calculated *DI*s from the two sensors before and after Damage 1 is introduced.

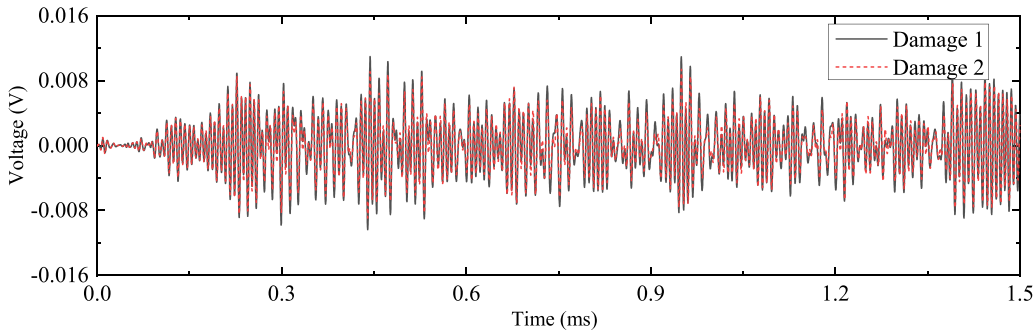

(a)

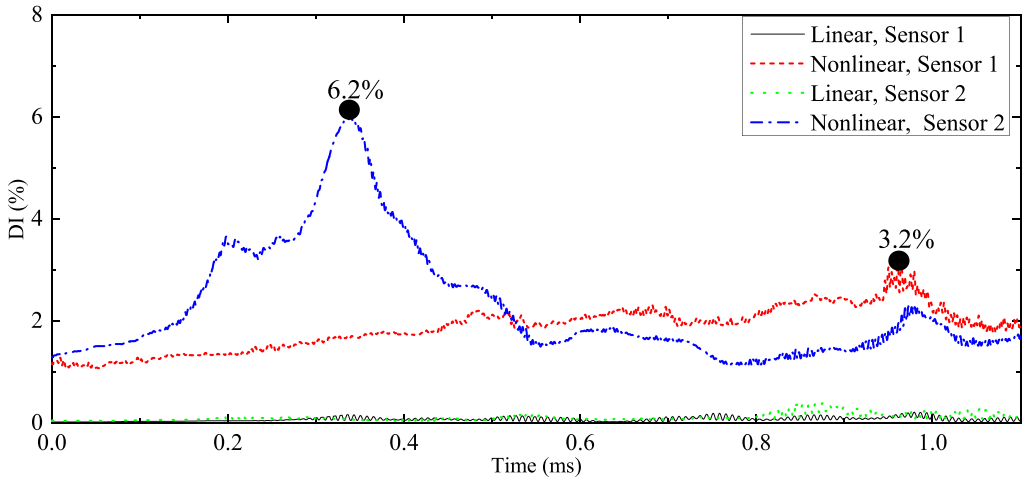

(b)

Figure 16. Responses of Sensor 1: (a) nonlinear response and (b) calculated *DI*s from the two sensors before and after the introduction of Damage 2.

5. Conclusions

Targeting the need for local incipient damage detection in complex structures, this work proposes a metamaterial-assisted nonlinear CWI (NGW-CWI) method. The designed meta-screen allows for the passing of the fundamental waves while stopping the second harmonic waves. This warrants the second harmonic signals received by the sensors, which are enclosed by the meta-screen, only stem from the interaction between the damage and the fundamental waves of the probing signals. Through customizing the geometry of the meta-screen and its layout to cover a specific monitoring zone, the second harmonic Lamb waves generated by the deceptive nonlinear sources are prohibited to enter the inspection area while the damage-induced nonlinear waves are confined inside the monitoring zone. As a result, the proposed method shows high sensitivity to local incipient damage and offers increased robustness against nonlinear interferences in the monitoring system.

As a very first attempt to combine the second harmonic Lamb waves and CWI, the proposed method shows great promise for practical implementation as a feasible solution for incipient damage monitoring in complex structures. Embracing the concept of metamaterials, the NGW-CWI method is significantly improved in terms of detection sensitivity and robustness. While the presented work is intended as a proof-of-concept study, the principle laid out in this paper is very generic which can be followed and extended to other integrated design of structures embedded with functional metamaterials/devices for local incipient damage monitoring purposes.

Data availability statement

The data cannot be made publicly available upon publication because no suitable repository exists for hosting data in this field of study. The data that support the findings of this study are available upon reasonable request from the authors.

Acknowledgments

The work was supported by Grants from the National Natural Science Foundation of China (12302114), the Research Grants Council of Hong Kong Special Administrative Region (PolyU 152013/21E), the Natural Science Foundation of Shanghai (22ZR1462700), the Fundamental Research Funds for the Central Universities and the Innovation and Technology Commission of the HKSAR Government to the Hong Kong Branch of National Rail Transit Electrification and Automation Engineering Technology Research Center (K-BBY1).

ORCID iDs

Shengbo Shan https://orcid.org/0000-0002-0950-6193
Ze Liu https://orcid.org/0000-0002-4565-4767
Li Cheng https://orcid.org/0000-0001-6110-8099

References

[1] Lissenden C J 2021 Nonlinear ultrasonic guided waves—principles for nondestructive evaluation *J. Appl. Phys.* **129** 021101
[2] Yu L and Tian Z 2013 Lamb wave structural health monitoring using a hybrid PZT-laser vibrometer approach *Struct. Health Monit.* **12** 469–83
[3] Amjad U, Yadav S K and Kundu T 2015 Detection and quantification of pipe damage from change in time of flight and phase *Ultrasonics* **62** 223–36
[4] Zima B and Kędra R 2020 Detection and size estimation of crack in plate based on guided wave propagation *Mech. Syst. Signal Process.* **142** 106788
[5] Matlack K H, Kim J-Y, Jacobs L J and Qu J 2015 Review of second harmonic generation measurement techniques for material state determination in metals *J. Nondestruct. Eval.* **34** 273
[6] Su Z, Zhou C, Hong M, Cheng L, Wang Q and Qing X 2014 Acousto-ultrasonics-based fatigue damage characterization: linear versus nonlinear signal features *Mech. Syst. Signal Process.* **45** 225–39
[7] Wang J, Shen Y, Rao D and Xu W 2021 Physical-virtual time reversing of nonlinear Lamb waves for fatigue crack detection and quantification *Mech. Syst. Signal Process.* **160** 107921
[8] Li W, Chen B and Cho Y 2020 Nonlinear feature of phase matched Lamb waves in solid plate *Appl. Acoust.* **160** 107124
[9] Gao G, Liu C, Hu N, Deng M, Chen H and Xiang Y 2020 Response of second-harmonic generation of Lamb wave propagation to microdamage thickness in a solid plate *Wave Motion* **96** 102557
[10] Srivastava A and Di Scalea F L 2009 On the existence of antisymmetric or symmetric Lamb waves at nonlinear higher harmonics *J. Sound Vib.* **323** 932–43
[11] Ishii Y, Biwa S and Adachi T 2018 Non-collinear interaction of guided elastic waves in an isotropic plate *J. Sound Vib.* **419** 390–404
[12] Metya A K, Tarafder S and Balasubramaniam K 2018 Nonlinear Lamb wave mixing for assessing localized deformation during creep *NDT&E Int.* **98** 89–94
[13] Wan X, Tse P, Xu G, Tao T and Zhang Q 2016 Analytical and numerical studies of approximate phase velocity matching based nonlinear S0 mode Lamb waves for the detection of evenly distributed microstructural changes *Smart Mater. Struct.* **25** 045023
[14] Zuo P, Zhou Y and Fan Z 2016 Numerical and experimental investigation of nonlinear ultrasonic Lamb waves at low frequency *Appl. Phys. Lett.* **109** 021902
[15] Sun X *et al* 2017 Simulations on monitoring and evaluation of plasticity-driven material damage based on second harmonic of S0 mode Lamb waves in metallic plates *Materials* **10** 827
[16] Ma C, Zhu W, Xiang Y and Zhang H (eds) 2017 Numerical and experimental investigations of nonlinear S0 Lamb mode for detection of fatigue damage *2017 IEEE Int. Ultrasonics Symp. (IUS)* (IEEE) (https://doi.org/10.1109/ULTSYM.2017.8092536)
[17] Shan S, Cheng L and Wen F 2018 Design of nonlinear-Lamb-wave-based structural health monitoring systems with mitigated adhesive nonlinearity *Smart Mater. Struct.* **27** 105006
[18] Planès T and Larose E 2013 A review of ultrasonic coda wave interferometry in concrete *Cem. Concr. Res.* **53** 248–55
[19] Snieder R, Grêt A, Douma H and Scales J 2002 Coda wave interferometry for estimating nonlinear behavior in seismic velocity *Science* **295** 2253–5

[20] Patra S and Banerjee S 2017 Material state awareness for composites part I: precursor damage analysis using ultrasonic guided coda wave interferometry (CWI) *Materials* **10** 1436
[21] Zhou D, Huo L, Chen D and Song G 2021 A feasibility study on monitoring of weld fatigue crack growth based on coda wave interferometry (CWI) *Smart Mater. Struct.* **30** 095013
[22] Gao F, Wang L, Hua J, Lin J and Mal A 2021 Application of Lamb wave and its coda waves to disbond detection in an aeronautical honeycomb composite sandwich *Mech. Syst. Signal Process.* **146** 107063
[23] Chen D, Shen Z, Fu R, Yuan B and Huo L 2022 Coda wave interferometry-based very early stage bolt looseness monitoring using a single piezoceramic transducer *Smart Mater. Struct.* **31** 035030
[24] Farin M, Moulin E, Chehami L, Benmeddour F, Nicard C, Campistron P, Bréhault O and Dupont L 2022 Monitoring saltwater corrosion of steel using ultrasonic coda wave interferometry with temperature control *Ultrasonics* **124** 106753
[25] Smagin N, Trifonov A, Matar O B and Aleshin V 2020 Local damage detection by nonlinear coda wave interferometry combined with time reversal *Ultrasonics* **108** 106226
[26] Qu S, Hilloulin B, Chupin O, Piau J-M, Abraham O and Tournat V 2023 Towards quantifying the effect of pump wave amplitude on cracks in the nonlinear coda wave interferometry method *Ultrasonics* **132** 106991
[27] Shan S, Cheng L and Li P 2016 Adhesive nonlinearity in Lamb-wave-based structural health monitoring systems *Smart Mater. Struct.* **26** 025019
[28] Lim H J, Lee H, Skinner T, Chattopadhyay A and Hall A 2021 Fatigue damage detection and growth monitoring for composite structure using coda wave interferometry *Struct. Control Health Monit.* **28** e2689
[29] Ciampa F, Mankar A and Marini A 2017 Phononic crystal waveguide transducers for nonlinear elastic wave sensing *Sci. Rep.* **7** 1–8
[30] Lott M, Roux P, Rupin M, Colquitt D and Colombi A 2021 Negative index metamaterial through multi-wave interactions: numerical proof of the concept of low-frequency Lamb-wave multiplexing *Sci. Rep.* **11** 1–8
[31] Tian Y, Song Y, Shen Y and Yu Z 2022 A metamaterial ultrasound mode convertor for complete transformation of Lamb waves into shear horizontal waves *Ultrasonics* **119** 106627
[32] Tian Y, Shen Y, Rao D and Xu W 2019 Metamaterial improved nonlinear ultrasonics for fatigue damage detection *Smart Mater. Struct.* **28** 075038
[33] Sherwood G R, Chronopoulos D, Marini A and Ciampa F 2021 3D-printed phononic crystal waveguide transducers for nonlinear ultrasonic damage detection *NDT&E Int.* **121** 102456
[34] Shan S, Wen F and Cheng L 2021 Purified nonlinear guided waves through a metamaterial filter for inspection of material microstructural changes *Smart Mater. Struct.* **30** 095017
[35] Liu Z, Shan S and Cheng L 2022 Nonlinear-Lamb-wave-based plastic damage detection assisted by topologically designed metamaterial filters *Struct. Health Monit.* **22** 1828–43
[36] Shan S, Liu Z, Cheng L and Pan Y 2022 Metamaterial-enhanced coda wave interferometry with customized artificial frequency-space boundaries for the detection of weak structural damage *Mech. Syst. Signal Process.* **174** 109131
[37] Ambroziński Ł, Magda P, Stepinski T, Uhl T and Dragan K 2014 A method for compensation of the temperature effect disturbing Lamb waves propagation *AIP Conf. Proc.* **1581** 1157–64
[38] Fendzi C, Rebillat M, Mechbal N, Guskov M and Coffignal G 2016 A data-driven temperature compensation approach for structural health monitoring using Lamb waves *Struct. Health Monit.* **15** 525–40
[39] Wang X, Niederleithinger E and Hindersmann I 2022 The installation of embedded ultrasonic transducers inside a bridge to monitor temperature and load influence using coda wave interferometry technique *Struct. Health Monit.* **21** 913–27
[40] Shan S and Cheng L 2022 Two-dimensional scattering features of the mixed second harmonic A0 mode Lamb waves for incipient damage localization *Ultrasonics* **119** 106554
[41] Tian Y and Shen Y 2020 Selective guided wave mode transmission enabled by elastic metamaterials *J. Sound Vib.* **485** 115566
[42] Choi G, Liu Y, Lissenden C J and Rose J 2014 Influence of localized microstructure evolution on second harmonic generation of guided waves *AIP Conf. Proc.* **1581** 631–8
[43] Wen F, Shan S and Cheng L 2022 Immunity of the second harmonic shear horizontal waves to adhesive nonlinearity for breathing crack detection *Struct. Health Monit.* **21** 2340–53